How Do Atmosphere and Land Surface Influence Seasonal Changes of Convection in the Tropical Amazon?

RONG FU, BIN ZHU, AND ROBERT E. DICKINSON

Institute of Atmospheric Physics, The University of Arizona, Tucson, Arizona

(Manuscript received 24 November 1997, in final form 9 June 1998)

ABSTRACT

Although the wet season in the tropical Amazon (10°N–20°S) at any one place and in any one year is initiated rapidly by synoptic systems, large-scale thermodynamic conditions modulate the frequency and intensity of these synoptic systems and hence control the climatology of the wet season. In this study, the satellite radiances, radiosondes, and assimilation data of the atmosphere are analyzed to show that the conditioning of the large-scale thermodynamics for the onset of the wet season is controlled by a moistening of the planetary boundary layer (PBL) and a lowering of temperature at its top, hence reducing convective inhibition energy (CINE). These changes occur either in phase with or lagging by one month the enhancement of low-level moisture convergence. Integration of a slab mixed-layer model shows how a higher humidity can reduce the drying effect of the entrainment and increase the humidity of the daytime PBL. Hence, the increase of low-level moisture convergence may provide enough moisture to initiate the wet seasons.

In the southern part of the basin (5°S–20°S), the land surface warming from austral winter to spring reduces the strong stability of the dry season and increases the frequency of unstable profiles for deep convection (f_{CUS}), but convection remains infrequent until, in addition, the PBL is moistened and the inversion decays to lower CINE in October. The latter occur one month after the moisture becomes convergent. The seasonal changes in land surface temperatures are stronger than those over the adjacent oceans and hence have more influence on the gradient between land and ocean, and so on the changes in the large-scale circulation.

In the equatorial western Amazon, a warmer land surface provides high f_{CUS} all year round, but the seasonal changes of convection are more controlled by CINE. In the eastern basin, a lower f_{CUS} in spring suppresses the expected wet season. Hence, convection is most frequent during austral fall, but also occurs in austral spring in the western Amazon. Higher f_{CUS} and lower CINE are largely contributed to by the increases in humidity and weakening of the inversion. In contrast to the southern part of the basin, changes in local land surface temperature are small so that changes of the surface temperature in the adjacent oceans and southern Amazon largely control the changes in temperature gradient between land and ocean, and hence the seasonal onset of equatorial convection.

1. Introduction

More than 80% of the precipitation over the Amazon is produced by atmospheric deep convection (Greco et al. 1990). Hence, an understanding of what controls the seasonal changes of this deep convection (hereinafter referred as convection) is needed to determine the seasonality of precipitation, and hence the effects on the latent and radiative forcing of the atmospheric circulation, and inputs to land surface processes. The latter is important for the ecosystems, agriculture, and water management in tropical South American countries.

Amazon rainfall occurs primarily in organized convective complexes. Seasonal variations of the frequency of those systems largely determine seasonality of monthly rainfall amounts. Their initiation requires not only a supply of available energy from their large-scale environment, as indicated by the convective available potential energy (CAPE) and the gross moist instability (Neelin 1997), but also dynamic conditions, such as rising motion and suitable wind shear, to efficiently release their environmental energy (Garstang et al. 1994; Cohen et al. 1995). On synoptic scales, instability to moist convection is necessary but not sufficient for the occurrence of organized convective complexes. However, on the seasonal scale the growth into organized convective systems of either easterly waves (Kagano 1979; Cohen et al. 1995) or intraseasonal oscillations (Knutson and Weickmann 1987; Jones and Weare 1993) depends probabilistically on how readily they can draw energy from their environment. Large-scale thermodynamic conditions determine the latter and, hence, their changes can modulate the frequency and strength of the convection. The wet season at any one place and in any

Corresponding author address: Rong Fu, Institute of Atmospheric Physics, The University of Arizona, 1118 E. 4th St., Rm. 542, P.O. Box 210081, Tucson, AZ 85721-0081.
E-mail: fu@air.atmo.arizona.edu

one year in the Amazon is initiated rapidly by synoptic events, but we show in this paper how this initiation is controlled by gradual increases of the large-scale static instability and humidity from the dry to wet season. Seasonally, the thermodynamic and dynamic processes are interdependent. For example, the establishment of a more humid and unstable thermal environment for moist convection is influenced by the wind fields, which advect moisture and destabilize the lapse rate adiabatically. We examine the hypotheses that the changes of the large-scale thermodynamic conditions facilitate the release of the potential (mainly latent) energy prior to and during the wet season and that the large-scale atmospheric circulation and the land surface conditions influence these changes and, hence, the onset of the wet season.

Seasonality of precipitation is influenced by the complex responses of the atmospheric circulation and of the land surface to the migration of the sun. Over the equatorial Amazon, although solar radiation at the top of the atmosphere peaks at the equinoxes, only a short wet season occurs in austral fall in the east, but a long wet season from austral spring to fall occurs in the west, for reasons that have not been clearly understood. Previous studies have emphasized either how large-scale atmospheric circulation or how land surface conditions can directly control the seasonal changes in convection. The studies invoking controls of convection by large-scale circulation emphasize the obvious relationship between the rapid establishment of the Bolivian high in the upper troposphere and moisture transport from the Atlantic Ocean (Marengo 1992; Rao et al. 1996) for initiation of the wet season (Kreuels et al. 1975; Virji 1981; Nishizawa and Tanaka 1983; Chu 1985). However, the 5-day composite circulation pattern around the onset of the wet seasons during 1985–86, as analyzed by Horel et al. (1989), implies the establishment of the Bolivian high follows the onset of convection and, hence, alternatively may be an effect of precipitation. Furthermore, model simulations suggest that the latent heat of the precipitation is necessary to produce the Bolivian high with realistic strength (e.g., Schwerdtfeger 1961; Figueroa et al. 1995; Lenters and Cook 1997). Evidently, whether or not the changes of circulation occur prior to the onset of convection has remained unclear.

Eltahir and Pal (1996) have shown that Amazon convection is closely related to the land surface wet-bulb temperature, in agreement with Williams's (1991) finding on a global scale, in which he has shown that wet-bulb temperature, an indicator of the surface air buoyancy, generally determines the amount of CAPE since the changes of the temperature aloft are mostly small. Elevation of the surface wet-bulb temperatures has often been argued in terms of an increase of surface temperature associated with an increase of insolation. However, changes of surface humidity can also change the wet-bulb temperature. Whether the elevation of surface wet-bulb temperatures at the end of dry season is provided largely by an increase of local sensible and latent fluxes from the land surface has been unclear. While such an increase is possible in a humid and weakly stable climate such as the tropical Amazon, the surface wet-bulb temperature could also be elevated by more humid air from the adjacent Atlantic Ocean that is entrained into the planetary boundary layer (PBL). None of these possibilities has been evaluated observationally.

Thus, past studies have helped clarify but not made obvious the thermodynamic contributions to the onset of the Amazon wet seasons and the role of atmospheric circulation and land surface conditions. Furthermore, how changes in circulation and land surface conditions affect the vertical buoyancy structure in addition to the amount of CAPE and what changes of the vertical thermodynamic structure influence convective instability have not been examined thoroughly for the Amazon region. Since convection over the Amazon will be generated by buoyancy and is parameterized according to the vertical profiles of buoyancy, answering these questions is a prerequisite to understanding how circulation, land surface conditions, and convection are related and how to better model the seasonal changes of convection.

This work addresses the above issues for the Amazon region by analyzing data from satellite radiances, radiosondes data, in situ surface micrometerological observations, and assimilation of atmospheric thermal and dynamic fields. By identifying changes in the vertical thermodynamic structure that have the most significant effect on the convective instability and then relating them to the changes in circulation and land surface conditions, we seek to systematically characterize how instability, circulation, and land promote an increase in the frequency of convection and, hence, the onset of the wet season in the Amazon.

2. Data and methods

The data used by this study include an International Satellite Cloud Climatology Project radiances (ISCCP B3) dataset, the National Centers for Environmental Prediction (NCEP) radiosonde data archived at the National Center for Atmospheric Research (NCAR) radiosonde dataset, radiosonde data from the joint Brazil–United States Amazon Boundary Layer Experiment (ABLE), surface micrometerological observations from the Amazon Region Micrometeorology Experiment (ARME), and a Goddard Earth Observing System Data Assimilation Office (GEOS-1) reanalysis monthly dataset. Convection is detected from the deep convective clouds (DCC) identified in the infrared (IR) images provided by the ISCCP B3 dataset (Rossow and Schiffer 1991), as analyzed for the period of April 1987–December 1993. To include the nonnegligible and seasonally varying contribution of nocturnal precipitation to the daily total precipitation (Velasco and Fritsch 1987; Greco et al. 1990), we calculate the daily mean frequency of DCC and hence minimize the bias due to

changes in the diurnal distribution of the DCC. The eight IR images per day are used to obtain a value for daily mean DCC.

The threshold of brightness temperature for DCC is tested for the Amazon region by comparing the temperature distribution of DCC with a more reliable daytime method that uses a visible–infrared threshold (Fu et al. 1990). A distinct break around 224 K is found, such that very few DCC (bright–cold in the visible and infrared images) occur at temperatures warmer than that and few cirrus clouds (dull–cold in the visible and infrared images) occur at colder temperatures. Hence, all the pixels with temperatures colder than the 224-K IR temperature threshold are classified as DCC pixels. Using the DCC pixels so identified, the fractional coverage index of DCC ($f_{\rm DCC}$) is computed as the number of DCC pixels normalized by the number of total pixels for each $0.5^\circ \times 0.5^\circ$ latitude–longitude cell. The eighth daily values of $f_{\rm DCC}$ are used to compute the daily mean $f_{\rm DCC}$ for the tropical Amazon region (20°S–10°N, 30°–85°W).

The NCEP–NCAR radiosonde global dataset provides profiles of geopotential height, temperature, dewpoint, and horizontal wind at more than 2000 upper-air stations (Gaffen 1996). Soundings from the Manaus (3°S, 60°W), Belém (1.5°S, 49°W), and Vilhena (12.7°S, 60°W) upper-air stations are used to represent the atmospheric thermodynamic structure in the central and eastern equatorial Amazon region and the southern Amazon region, respectively.

Research-quality radiosondes that were launched every 3 h from 0800 to 1700 local time (LT) during ABLE (Harriss et al. 1988; Harriss et al. 1990) are also used to examine the evolution of the atmospheric thermodynamic structure from 0800, when most of the operational radiosonde data are obtained, to 1400 LT, when convection peaks diurnally. ABLE was conducted during the dry season from 15 July to 5 August 1985 (phase 2A) and during the wet season from 1 April to 15 May 1987 (phase 2B) to provide intensive observations of the atmospheric chemical and dynamic processes. These radiosondes are from Reserve Ducke (2°56′S and 59°57′W, 90 m above mean sea level), 20 km northeast of Manaus during the phase 2A, and from Embrapa (2°56′S and 60°01′W, 78 m above mean sea level), 7 km west of Reserve Ducke during the 2B phase of ABLE (Garstang et al. 1990).

The vertical profiles are linearly interpolated to 10-mb increments from the surface to 700 mb and to 50-mb increments from 700 to 100 mb, according to the data sampling and to resolve changes that affect convection. Potential temperature (θ), equivalent potential temperature (θ_e), and saturation equivalent potential temperature ($\theta_{\rm es}$) are computed by considering the temperature and humidity dependence of latent heat using Bolton's (1980) formulas, as explained in more detail in Fu et al. (1994). Buoyancy that surface air would have when it convects (hereafter referred to as buoyancy without mixing with its environmental air) and negative buoyancy of the atmosphere below the level of free convection (LFC), referred to as convective inhibition energy (CINE), are computed from the instantaneous radiosonde profiles with consideration of both latent heat of freezing and condensation loading (Williams and Rennó 1993). The sensitivity tests with reversible moist-adiabatic and psedoadiabatic assumptions show little dependence of CINE on the assumptions used in its computation.

ARME (Shuttleworth 1988) provides hourly measurements of surface solar and net radiative fluxes, sensible and moisture fluxes, and wind, etc., at the Reserve Ducke, that is, collocated in space with the radiosonde measurements of ABLE 2A for the period of September 1983–September 1985. The GEOS-1 reanalysis data (Schubert et al. 1993) are used for monthly and daily mean temperature, humidity, the pressure at the surface and in the atmosphere, the lower-tropospheric winds, the moisture transport and convergence, and geopotential height at 200 mb to provide diagnoses of large-scale thermal and dynamic properties of the atmosphere and land surface.

A simple slab mixed-layer model (Tennekes 1973; Betts 1973) helps infer the temperature and humidity in the afternoon planetary boundary layer (PBL) from the morning radiosondes and evaluate the relative importance of the surface moisture flux and the moisture flux at the top of the PBL to the seasonal changes of the humidity in the PBL. Martin et al. (1988) tested it for the ABLE 2A region using tethered balloon, radiosonde, and aircraft ultraviolet differential absorption lidar and found that the horizontal advection is negligible. It is simplified to

$$\frac{\partial \theta}{\partial t} = \frac{\rho(\overline{\omega'\theta'_s} - \overline{\omega'\theta'_h})}{h} \tag{1}$$

$$\frac{\partial q}{\partial t} = \frac{\rho(\overline{\omega'q'_s} - \overline{\omega'q'_h})}{h}, \tag{2}$$

where q is the specific humidity of the PBL, h its height, ρ the air density, $\overline{\omega'\theta'_s}$ and $\overline{\omega'q'_s}$ the surface fluxes of sensible and moisture heat obtained from the hourly observations at Reserve Ducke, and $\overline{\omega'\theta'_h}$ and $\overline{\omega'q'_h}$ the sensible heat and moisture flux at the top of the PBL. The latter are computed by

$$\overline{\omega'\theta'_h} = W_{\rm ent}(\theta_u - \theta_d) \tag{3}$$

$$\overline{\omega'q'_h} = W_{\rm ent}(q_u - q_d), \tag{4}$$

where $W_{\rm ent} = dh/dt - W_e$ is the entrainment velocity, dh/dt is the growth rate of the PBL height, and W_e is the environmental subsidence. The subscripts u and d denote above and below the top of the PBL, respectively. Simulations with this simple mixed layer model agree with the ABLE 2A observations for the potential temperatures and humidity in the PBL and at the surface preceding the start of moist convection around 1300 (Martin et al. 1988).

Section 3 details how seasonal changes of convection vary geographically between the eastern and western equatorial basins (4°N–6°S) taken to be divided at 60°W and for the southern basin (6°S–20°S). The onset of convection in each of the above regions is separately discussed.

3. Results

Convection over the Amazon Basin generally peaks in mid- to late afternoon whereas data from operational radiosondes are mostly available only for 0800 LT at Manuas and Vilhena and for 0840 LT at Belém. ABLE radiosonde data, as detailed in section 3a, link the morning soundings to the afternoon convection. The transition of the vertical thermodynamic structure between the dry and wet seasons is analyzed in section 3b to determine how these changes affect convection. How changes in large-scale circulation and in land surface temperature and humidity affect the vertical buoyancy profiles and hence convection is examined in section 3c.

a. Diurnal variations suggested by ABLE soundings

How the profiles of θ, θ_e, and θ_{es} evolve from morning to afternoon are analyzed using radiosonde temperature and humidity data from ABLE. Figure 1 shows mean profiles of 0800 (Fig. 1a), 1100 (Fig. 1b), 1400 (Fig. 1c), and 1700 (Fig. 1d) LT at Reserve Ducke for the dry season ABLE 2A. The θ_{es} profile indicates that an early morning layer that is stable below 950 mb is destabilized by 1100 LT. The layer is again stabilized by cooling near sunset (1700 LT). The midday buoyancy destabilization is mainly through the increase in the surface temperature. Changes of θ_{es} from 0800 to 1700 LT above the 950-mb level were less than 5 K, compared to the 18 K at the surface. Mixing with drier air entrained at the top of the PBL as it grows in height from morning to early afternoon (Fitzjarrald and Garstang 1981; Martin et al. 1988) decreases boundary layer humidity and compensates for the effect of surface warming on θ_e. Hence, θ_e at 1000 mb remains constant at 350 K from 0800 to 1400 LT. The vertically integrated buoyancy and CINE at 1400 LT appear to be determined approximately by the profiles of θ_e and θ_{es} at 0800 LT, corrected for the changes of near-surface temperature and humidity. The LFC is 200–300 m higher than the mean top of the PBL [located at 0.8 km and 1.2 km at 1100 and 1400 LT, respectively, as measured by lidar and tethered balloons; Martin et al. (1988)] and CINE is about 13 J kg^{-1} at 1100 LT and 10 J kg^{-1} at 1400. Hence, the turbulence within the PBL is on average too shallow to initiate local deep convection, and initial vertical velocity has to be greater than 5 m s^{-1} at 1100 and 4.5 m s^{-1} at 1400 LT or, equivalently, values of low-level convergence have to be greater than 6.4×10^{-3} s^{-1} and 3.8×10^{-3} s^{-1} (according to the above-observed PBL depths), respectively, in order to overcome the initial negative buoyancy.

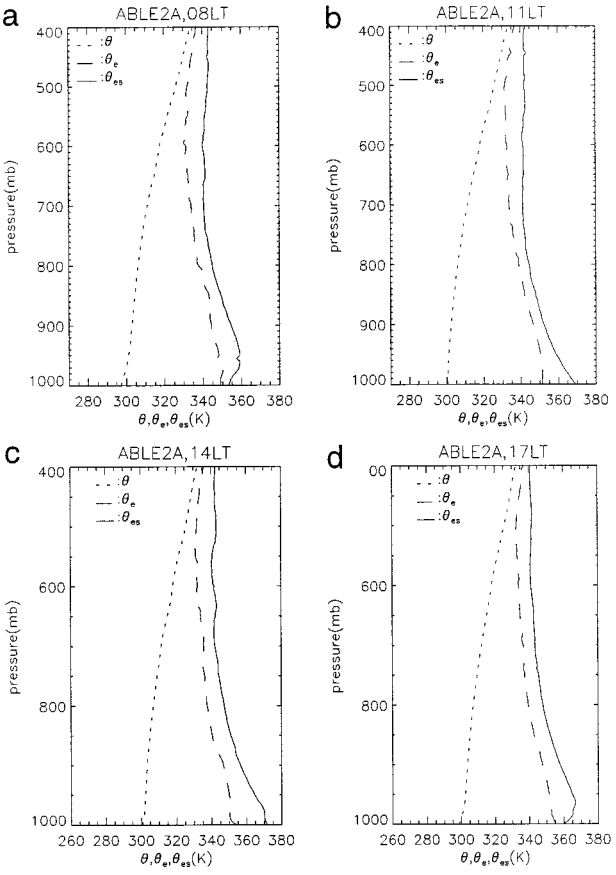

FIG. 1. Profiles of θ, θ_e, and θ_{es} at Reserve Ducke (2°56′S, 59°57′W) averaged for the period of ABLE 2A (15 Aug–5 Sep 1985) at (a) 0800, (b) 1100, (c) 1400, and (d) 1700 LT.

The ABLE 2B wet season profiles (Fig. 2) in early morning start with comparable θ_e as in the dry season, but initially lower temperatures at overlying levels, and a correspondingly lower θ_{es} (5 K lower at 950 mb). Evidently, the wet season PBL is slightly colder but more humid than those of the dry season as shown in Fig. 3. By late morning (1100), θ_e at both the surface and at 950 mb has come closer to θ_{es} because of increasing humidity and is consequently 3 K warmer at the surface than in the dry season; whereas surface temperature and, hence, θ_{es} continue to resemble those of the dry season through early afternoon (1400 LT). By late morning, the profile is destabilized by the higher θ_e at 1000 mb with the lower θ_{es}; the top of the PBL has risen above the LFC by 1100 LT and remains so into the afternoon (Browell et al. 1990). Compared to the dry season, the CINE is reduced by more than 8 J kg^{-1}. An initial velocity greater than 3 m s^{-1} or, equivalently, 3×10^{-3} s^{-1} in convergence below 1 km is required to overcome the CINE. Since the negative energy barriers are only one-half of that of the dry con-

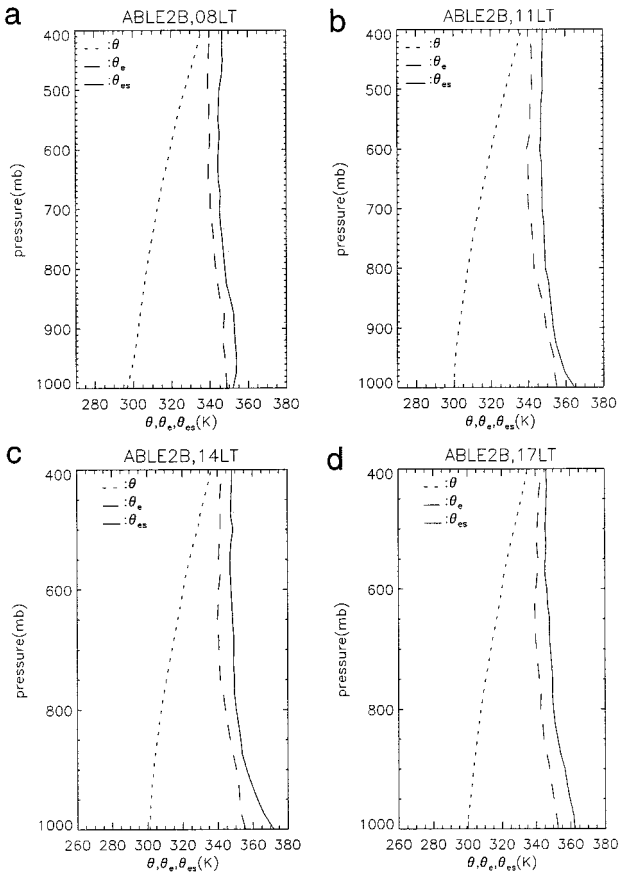

FIG. 2. As in Fig. 1 but at Embrapa (2°56′S, 60°01′W) for the period of ABLE 2B (1 Apr–15 May 1987).

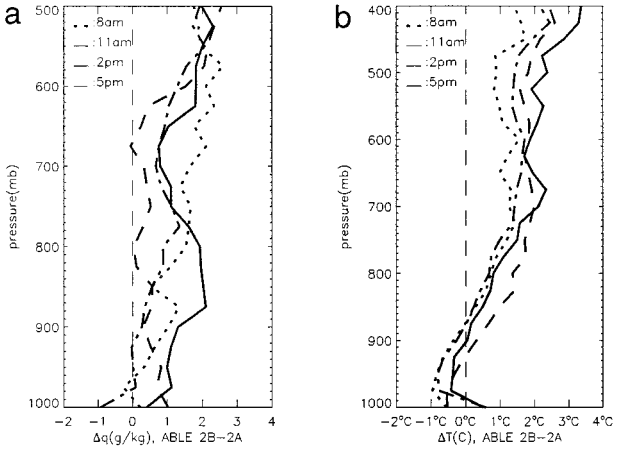

FIG. 3. (a) The profiles of the mixing ratio of water vapor averaged over the ABLE 2B period minus those for the ABLE 2A at 0800, 1100, and 1400 LT, respectively. The unit is g kg^{-1}. (b) As in (a) but for temperature with units of °C.

dition during ABLE 2A, convection is more easily initiated.

For the weak advection in the PBL found during ABLE (Martin et al. 1988), there are two possible providers of this increased wet season moisture: a relatively higher moisture flux at the surface or a moisture entrainment at the top of the PBL. At the peak of the wet season, as shown in Fig. 2, both processes may be responsible for the higher humidity at 1400 LT. But entrainment would be a more likely initiator of the wet season for the relatively small moisture flux at the end of dry season compared to that during the wet season. The importance of the entrainment and the initial humidity in the PBL at 0800 LT is tested by a pair of simulations using the PBL model described in section 2. The first of these simulates the growth of the dry season PBL from 0800 to 1400 LT. We use the ABLE radiosondes at 0800 LT to establish initial conditions for θ, q, θ_u, θ_d, q_u, and q_d, then drive the model with the surface sensible and moisture fluxes ($\overline{\omega'\theta'_s}$ and $\overline{\omega'q'_s}$) and horizontal winds measured by ARME, which coincide with ABLE 2A. The growth rate ($W_{\text{ent}} = dh/dt - W_e$) of the PBL is set to 8 cm s^{-1} according to the airborne ultraviolet differential absorption lidar observations from ABLE 2A, so that the averaged dh/dt from 0800 to 1300 LT is 8 cm s^{-1} but that W_e is zero before 1400 LT. Updates of θ_u and q_u are provided by the ABLE radiosonde measurements at 1100 and 1400 LT. The terms θ_d and q_d are the same as θ and q, and are computed from Eqs. (1) and (2) after 0800 LT.

The second simulation is initiated from the same dry conditions shown in Fig. 1a and driven by the same dry season surface fluxes and entrainment velocity as in the first experiment. Thus, the differences in PBL conditions at 1400 LT between the two simulations are caused only by the differences in temperature and humidity above the PBL between the dry and wet seasons. As illustrated in Fig. 4, the mixed-layer humidity at 1300 LT is 0.5 g kg^{-1} higher in the second simulation. Since the observed mixed-layer humidity is 1 g kg^{-1} higher for ABLE 2B than for ABLE 2A, these simulations suggest

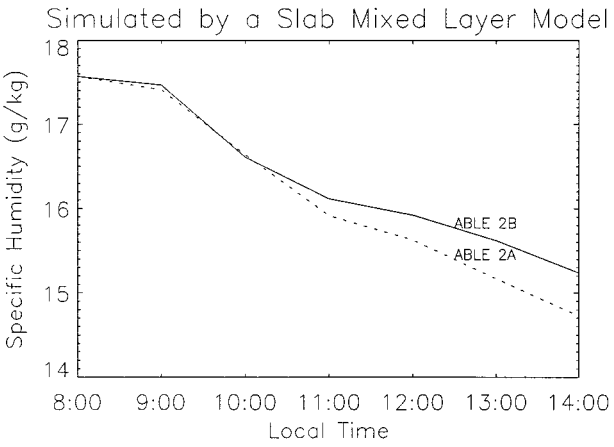

FIG. 4. Specific humidity of the mixed layer between 0800 and 1400 LT computed by the simple slab mixed-layer model. The dry curve is initiated from the averaged temperature and humidity profiles at 0800 from ABLE 2A, and the wet curve is from ABLE 2B.

that more than half of the seasonal changes of humidity in the early afternoon of the mixed layer are contributed to by differences in the humidity of entrained air at the top of the mixed layer, consistent with the more comprehensive evaluation of the mixed-layer structure for ABLE 2A (e.g., Martin et al. 1988). The observed difference is presumably accounted for by the dry season initial PBL humidity and evaporation used here being lower than during the wet season and by the use of the same boundary layer growth rate. Since the mixed-layer humidity increase required to initiate the wet season is likely smaller than what has been reached by the peak of the wet season, this simple analysis suggests that the increase of humidity above the PBL provides more than half of the humidity increase in the PBL needed for initiating the wet season.

b. How the environmental vertical thermodynamic structure relates to the onset of convection

Although Eltahir and Pal (1996) suggested a positive correlation between the occurrence of convection and CAPE in the Amazon Basin, based on 2-yr surface wetbulb temperature and rain gauge data at Reserve Ducke (Shuttleworth 1988), convection does not necessarily occur when CAPE exists. Other factors such as CINE and proper dynamic conditions are also likely to control the occurrence of convection (Williams and Rennó 1993; Fu et al. 1994). Dynamic conditions providing organized low-level convergence lift the near-surface air and hence destabilize the lapse rate adiabatically and moisten the low troposphere. The latter two effects are included in an analysis of the vertical buoyancy structure. Approximately 6 yr of radiosonde data are used here to examine the seasonal changes of instability and CINE and what causes these changes.

Deep convection requires a deep layer of positive or neutral buoyancy. When radiosonde profiles indicate such a layer extending from 850 mb to at least 400 mb (or at least from 800 mb to 400 mb at Vilhena due to higher elevation), we refer to the sounding as a convectively unstable sounding. The frequency of the convectively unstable soundings (f_{CUS}) is computed by the number of such soundings normalized by the number of total available soundings. The morning soundings underestimate buoyancy and overestimate CINE compared to what radiosondes in the early afternoon would give. At Vilhena in the south-central Amazon (Fig. 5a), f_{CUS} is more than 20% in January and February and less than 3% during July and September. The June–September minimum of f_{DCC} is generally out of phase with CINE if the undersampled July is excluded. CINE is minimum (25 J kg^{-1} or less) during December–March when f_{DCC} is maximum, and maximum (30–60 J kg^{-1}) during June–September when f_{DCC} is minimum. Thus, the atmosphere is more frequently unstable and convecting parcels work against less initial resistance during the wet season than during the dry. The probability

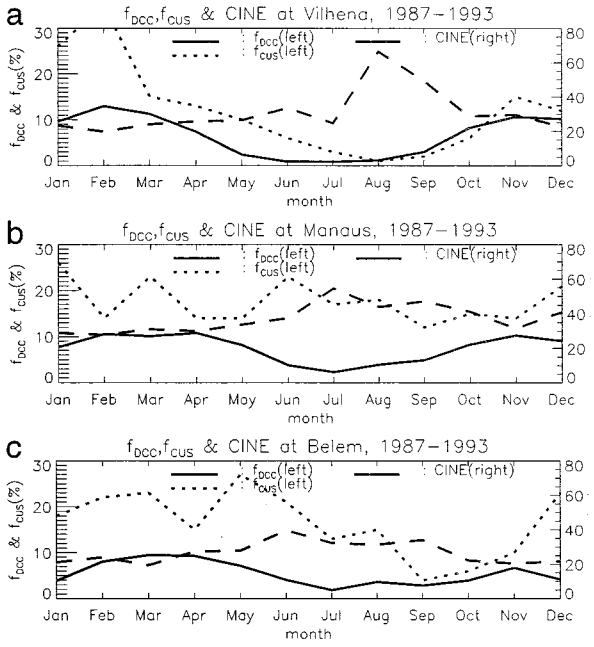

FIG. 5. (a) Averaged annual changes of f_{DCC} for a 1° × 1° lat–long square centered at Vilhena (solid curve, left ordinate) and f_{CUS} (dotted curve, left ordinate) and CINE of the convectively unstable soundings at Vilhena (dashed curve, right ordinate) for the period of Jan 1987–Dec 1993. (b) As in (a) but for Manaus in the central equatorial Amazon. (c) As in (a) but for Belém in the eastern equatorial Amazon.

for dynamic disturbances or boundary layer thermals to develop increases as the probability of unstable conditions increases and the amount of CINE decreases.

Important differences in the equatorial Amazon between Manaus and Belém are seen by comparing Figs. 5b and 5c. The Manaus soundings (Fig. 5b) show an f_{CUS} that is greater than 14% for all months and that it does not correlate with f_{DCC} and, thus apparently does not act to inhibit convection. By contrast, f_{CUS} at Belém (Fig. 5c) is 10% or less from September to November, evidently suppressing convection in the austral spring. At Manaus, the relatively low values of CINE (30–40 J Kg^{-1}) from November to April presumably account for the maximum f_{DCC} during that period. At Belém, on the other hand, it appears to be the higher values of CINE from April to September that confine the occurrence of maximum DCC to the austral autumn.

Why f_{CUS} and CINE change to control the initiation of the wet season is examined in terms of the evolution of the profiles of θ_e and θ_{es} from the dry season to the wet season for 1987–93 in Figs. 6–11. At Vilhena (Fig. 6), July θ_e at the surface is colder than θ_{es} throughout the troposphere so that the atmosphere is stable. In January, on the other hand, a deep layer of positive buoyancy appears between 750 and 250 mb due to surface warming and moistening (Fig. 7), and there is little near-surface inversion at 0800 LT. Similar significant changes from dry to wet seasons are seen at Manaus and Belém (Figs. 8–11).

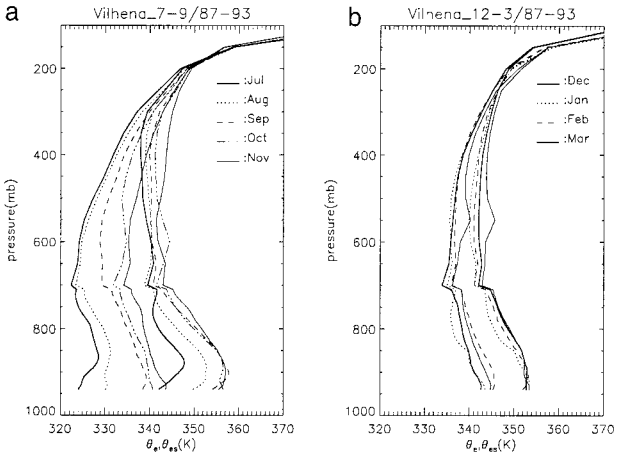

FIG. 6. (a) Evolution of the monthly profiles of θ_e and θ_{es} at Vilhena from Jul to Nov averaged over the period of 1987–93. The same types of curves are used for both θ_e and θ_{es} profiles for the same month as labeled in the upper-left corner of the diagram. (b) As in (a) but for Dec to Mar.

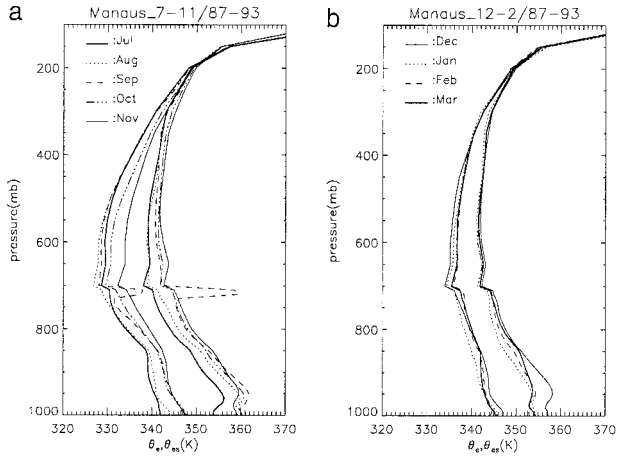

FIG. 8. (a) As in Fig. 6a but at Manaus in the central equatorial Amazon. (b) As in Fig. 6b but at Manaus.

These changes develop seasonally as follow. From July to August (Figs. 6a and 7a), θ_{es} (temperature) increases by about 5 K (2 K) below 700 mb while retaining a strong inversion above 900 mb. The layer between 800 and 500 mb begins to moisten although the PBL remains as dry as in July (Fig. 7b). From August to September, the warming below 700 mb continues, and the atmosphere becomes more humid (Fig. 7b), so differences between θ_e and θ_{es} are reduced (Fig. 6a). Although the buoyancy is consequently increased, convection is still discouraged by a strong stable PBL and an inversion (Fig. 6a), which contributes to a relatively large CINE (Fig. 5a). From October on (Fig. 6b), cooling destabilizes the inversion and the lapse rate becomes nearly moisture adiabatic. Humidity continues to increase and after November near-surface warming ceases (Fig. 7b). These changes provide the downward trend of CINE and upward trend of f_{CUS}, allowing the increases in DCC signaling increased convection (Fig. 5a).

The morning PBL at Manaus in July at mid–dry season shows a strong inversion in θ_{es} at 850 mb (Fig. 8a) that gradually erodes through September as the surface warms up more than the overlying layers (Fig. 9a). A jump in temperature is seen in August and continues through September. Consequently, CINE declines for the next several months (Fig. 5b). Starting from October, the surface layers become cooler and the 950-mb air decreases in temperature even more (Fig. 9). The lapse rates from September to November (Fig. 8a) are nearly as unstable as those from January to March (Fig. 8b), but the lower relative humidity in the morning implies a higher midafternoon LFC as inferred from the ABLE 2B diurnal cycle (Fig. 2). The LFC is near or above the

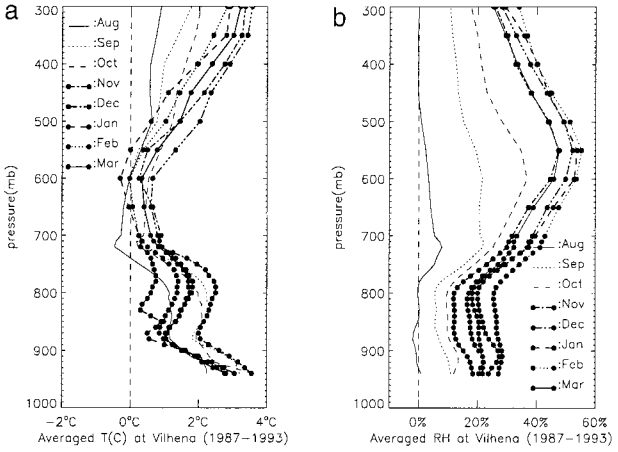

FIG. 7. (a) The seasonal changes of the monthly temperature profiles at Vilhena from Aug to Mar relative to that of Jul. The profile for each month is averaged for the period of 1987–93. The months of wet season are marked by dots. (b) As in (a) but for the mixing ratio of water vapor.

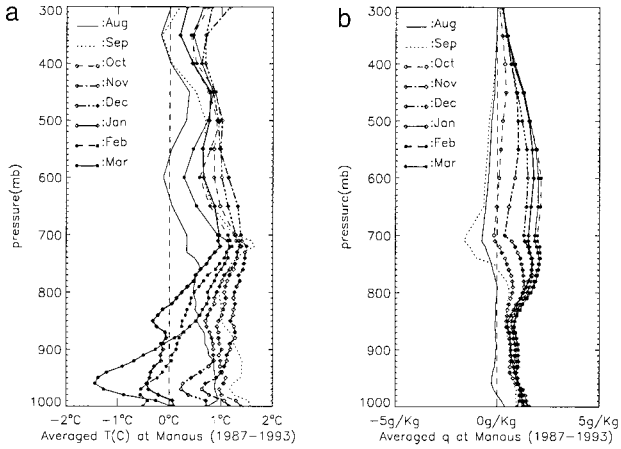

FIG. 9. As in Fig. 7 but for Manaus. The months of the wet season are marked by diamonds and the peak months are marked by dots.

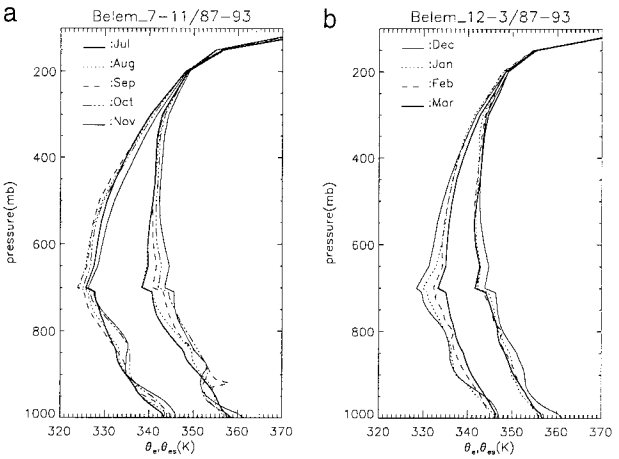

FIG. 10. As in Fig. 8 but for Belém in the eastern equatorial Amazon.

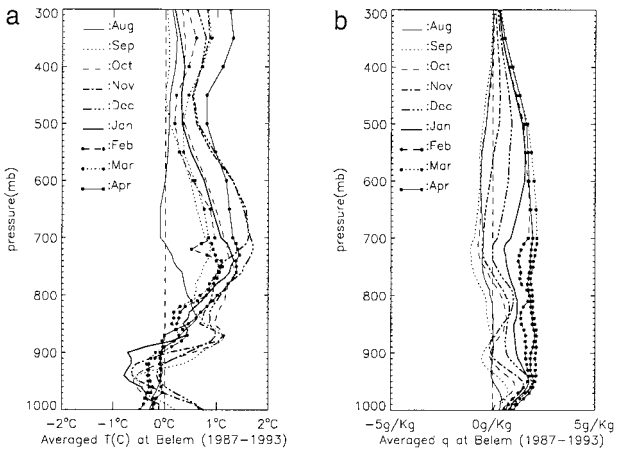

FIG. 11. As in Fig. 7 but for Belém.

averaged top of the afternoon PBL, which is around 860 mb in the former period but lowers to 900 mb over the latter period. Thus, the earlier period (October–January) can support convection on days when the PBL is higher than normal whereas over the latter period (February–March), most days can support convection. Hence, there is relatively less f_{DCC} and precipitation in the earlier period than in the latter period.

The moistening below 750 mb starts in September, lagging the increase of temperature but leading the onset of the wet season. Since the daily maximum PBL is usually shallower than 850 mb, the moistening above 850 mb must come either from an increase in the upward moisture transport out of the PBL or from a stronger horizontal moisture transport. Prior to the wet season, the surface evapotranspiration is usually low and convection that breaks through the PBL is infrequent. Furthermore, evaporation of clouds and precipitation would provide cooling, rather than the warming indicated by the temperature profiles in Fig. 9a. Hence, the increase of local evapotranspiration and upward moisture transport alone is evidently not enough to explain the observed moistening, but rather enhancement of horizontal moisture transport may contribute substantially to the increase of moisture in the lower troposphere. By contrast, during the wet season (October–January), the temperature below 700 mb decreases as the humidity increases with time, suggesting that evaporation of clouds and precipitation provide moisture during that period.

At Belém, from August to October (Fig. 10a), although the near-surface temperatures increase slightly, the warming between 900 and 850 mb clearly enhances the inversion at the top of the PBL. The associated decreases of relative humidity suggest that this is a result of a subsidence from 550 mb to the top of the PBL. The strengthening of the inversion weakens the mixing between the PBL and the atmosphere above it. Consequently, the PBL becomes more humid and unstable. From January on, the inversion is weakened, the entire troposphere column becomes more humid, and f_{CUS} is high (Fig. 5c) until April.

In summary, the seasonal onset of convection, as represented by an increase of the frequency of convection, responds in the southern Amazon to both the reduction of CINE and to the increased f_{CUS}. The surface warming and moistening from July to October destabilize the atmosphere, as shown in Fig. 5a, but convection does not occur until CINE becomes small in November and December. During this period, surface temperatures remain unchanged, but further increases in humidity destabilize the PBL and reduce CINE. In the equatorial basin, the lower f_{CUS} due to the weakening of the inversion during the austral spring in the eastern part suppresses convection. Otherwise, buoyancy is generally available, and CINE appears to control the seasonal changes of convection. From dry austral winter to spring, surface warming and moistening reduce CINE in the western equatorial Amazon, starting a wet season in that region. From austral summer to fall, the surface-air temperature decreases, but higher relative humidity in the lower troposphere and destabilization of the temperature profile in the PBL reduce CINE, providing a suitable large-scale environment for the onset of the primary wet season in austral fall.

c. The relationship between large-scale circulation, land surface temperature, vertical thermodynamic structure, and convection

How large-scale circulation and surface conditions together determine the vertical buoyancy structure and affect convection is examined in this section. The mean spatial patterns of the DCC, the geopotential height at 200 mb ($Z_{200\mathrm{mb}}$), and the averaged wind below 850 mb, as shown in Fig. 12 for July, October, January, and March provide a large-scale spatial background for the radiosonde results in Figs. 6–11. The DCC (shaded areas with $f_{\mathrm{DCC}} > 3\%$) in July (Fig. 12a) are confined to the

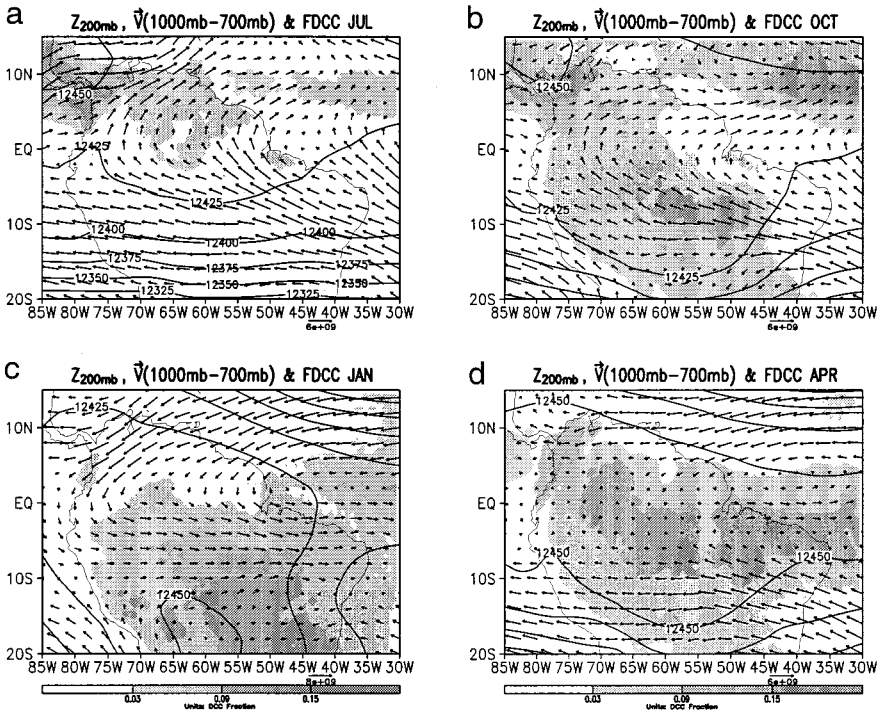

FIG. 12. Maps of f_{DCC} (shading), $Z_{200\mathrm{mb}}$ (contours), and averaged horizontal wind from surface to 700 mb (vectors) for (a) Jul, (b) Oct, (c) Jan, and (d) Apr, averaged over the period 1987–93. The unit of f_{DCC} is a fraction. The scale of the shade is indicated by the gray bar below the two bottom diagrams. The unit for $Z_{200\mathrm{mb}}$ is m and for wind is m s^{-1}.

areas north of the equator. The basin-wide average of f_{DCC} is 3%. It reaches 9% in the northern end of the basin and 15% in the eastern Pacific intertropical convergence zone (ITCZ) area. In October (Fig. 12b), DCC spreads over the entire Amazon Basin from 10°N to 15°S. But in the adjacent eastern Pacific and western Atlantic, convection is still confined to north of 5°N. No convection appears over the southern oceans or over the eastern basin within 10° in longitude of the east coast of South America and south of 5°N. In January (Fig. 12c), convection spreads over the entire Amazon Basin south of the equator, and f_{DCC} increases to 9%–15% over the central basin and over northeast Brazil. The DCC in the Atlantic ITCZ move to the equatorial area, and those of the eastern Pacific ITCZ fade out. In April (Fig. 12d), the DCC in the Atlantic ITCZ finally catch up with those over land and form an intensified zone between 0° and 10°S in the central to eastern Amazon and over the Atlantic Ocean. In the western Amazon, DCC have spread to north of the equator and the northeastern Pacific ITCZ begins to again establish itself.

Figures 13 and 14 show the temporal correlation between the seasonal changes of DCC and changes of surface temperature, humidity, the averaged wind below 850 mb, and $Z_{200\mathrm{mb}}$. In the southern basin (Fig. 13), surface temperatures usually are warmest around October at the beginning of the wet season (Fig. 13a) and then decrease quickly, consistent with the results of radiosonde observations at Vilhena (Fig. 5a). Coolest surface temperatures occur from the end of the wet season to about 1 or 2 months before the next wet season. Surface humidity (Fig. 13b) and $Z_{200\mathrm{mb}}$ (Fig. 13c), however, are both positively correlated to f_{DCC}. In the equatorial basin (Fig. 14), f_{DCC} peaks annually between January and April in the eastern part, following the changes of the surface humidity and $Z_{200\mathrm{mb}}$. Surface temperatures likewise peak before the beginning of the wet season, then drop to minimum values during the wet season, hence correlating to DCC in the same way as do these in the southern Amazon, although their seasonal range is only about half as great. In the western basin, the wet season begins in October and ends in April with high f_{DCC} in most years. Surface humidity, $Z_{200\mathrm{mb}}$, and f_{DCC} begin to increase in austral spring, about 3 months earlier than they do in the eastern basin, and surface temperatures likewise peak in September at the beginning of the f_{DCC} increase. The surface warming ceases as f_{DCC} increases, but the surface remains moderately warm until January when its temperature begins to decline to seasonally low values.

The links between the above seasonal distributions of convection and those of the large-scale airflow patterns have been discussed extensively in previous studies (e.g., Virji 1981; Kousky 1988; Horel et al. 1989; Hasternrath 1997; Garreaud and Wallace 1998). Here we

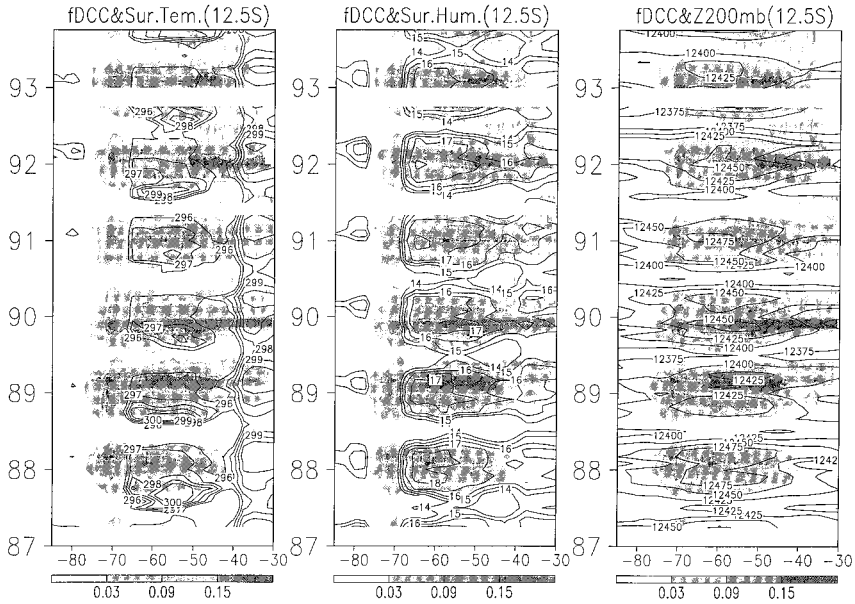

FIG. 13. (a) Hovmöller diagram of f_{DCC} (shading) and surface temperatures (contours) in K at 15°S between 30° and 85°W (abscissa) for the period of Jan 1987–Nov 1993 (ordinate). (b) As in the left panel but for surface specific humidity (contours in g kg^{-1}). (c) As in the left panel but for Z_{200mb} (contours) in m.

emphasize how these circulation changes affect the vertical buoyancy structure and, hence, convection. Figure 7 indicates that the increases of surface temperature from July to October destabilize the lapse rate below 900 mb in the southern Amazon but do not reduce CINE (Fig. 5a). Hence, the increase of surface temperature alone cannot initiate convection. However, the increases of surface humidity from October to December do reduce CINE (Fig. 5a), just preceding the seasonal onset of convection. Higher values of Z_{200mb}, probably driven by latent heating from moist convection (e.g., Lenters and Cook 1997), are generally associated with a large-scale rising motion. As shown by θ_{es} profiles in Fig. 6, cooling at 900 mb from November to December further reduces CINE, probably a consequence of the upward motion driven by the moist convection.

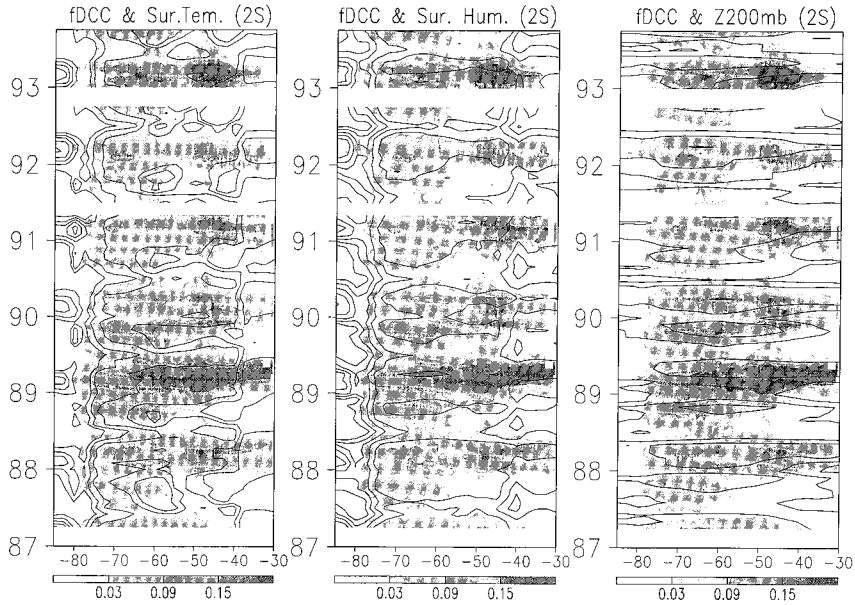

FIG. 14. As in Fig. 13 but for 2°S.

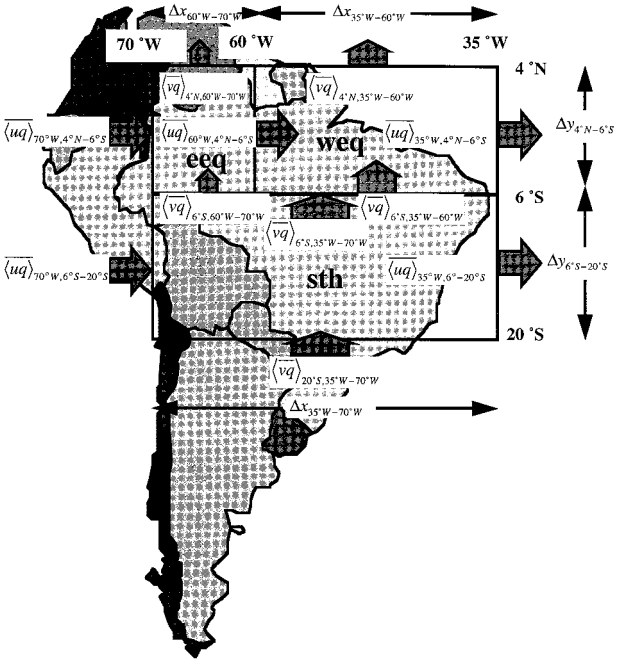

FIG. 15. Schematic diagram of the terms used in calculating moisture transport and convergence for the southern Amazon, the western equatorial Amazon, and the eastern equatorial Amazon.

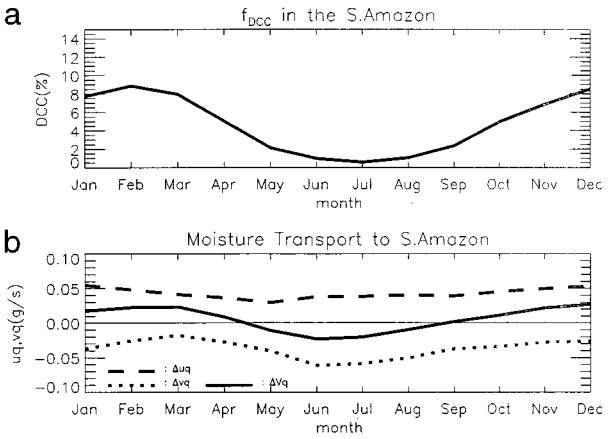

FIG. 16. (a) Climatological annual changes of f_{DCC} averaged over the southern Amazon Basin (6°–20°S, 35°–70°W) obtained from the period of 1987–93. (b) Climatological annual changes of $\langle \overline{\mathbf{V}q} \rangle_{sth}$ (solid curve), $\langle \overline{uq} \rangle_{sth}$ (dashed curve), and $\langle \overline{vq} \rangle_{sth}$ (dotted curve) for the period of 1987–93.

Changes in large-scale circulation also affect moisture transport. The correlation between moisture transport and the onset of the wet season has been examined in previous studies (e.g., James and Anderson 1984). However, it was not established whether the increase in moisture transport causes the wet season or rather is a consequence of convergence driven by the latent heat of precipitation. The results of Figs. 6–11 suggest that the moistening of the lower and middle troposphere starts prior to the onset of the wet seasons. We examine (Figs. 16–18) the changes of the moisture convergence and whether or not it causes the observed moistening in the Amazon Basin, as diagnosed by the terms illustrated in Fig. 15. Figure 16 shows the 6-yr averaged annual changes of the moisture transport to the southern Amazon region assimilated by GEOS-1. The net zonal moisture convergence to the southern Amazon Basin ($\Delta\langle \overline{uq} \rangle_{sth}$) is computed from

$$\Delta\langle \overline{uq} \rangle_{sth} = \frac{(\langle \overline{uq} \rangle_{70°W,6°S–20°S} - \langle \overline{uq} \rangle_{35°W,6°S–20°S})/\Delta y_{6°S–20°S}}{\Delta x_{35°W–70°W}}, \quad (5)$$

where $\langle \overline{uq} \rangle_{70°W,6°S–20°S}$ is the zonal moisture fluxes integrated from the surface to 700 mb and from 6° to 20°S along 70°W, and $\langle \overline{uq} \rangle_{35°W,6°S–20°S}$ is the same as $\langle \overline{uq} \rangle_{70°W,6°S–20°S}$ but along 35°W (Fig. 15). These two terms are normalized by the latitudinal distance between 6° and 20°S, denoted as $\Delta y_{6°S–20°S}$, such that the numerator represents the averaged net zonal fluxes per meter of latitudinal distance integrated from the surface to 700 mb. Here $\Delta x_{35°W–70°W}$ is the longitudinal distance between 35° and 70°W. A positive value of $\Delta\langle \overline{uq} \rangle_{sth}$ represents a net zonal moisture convergence in the region. The meridional moisture convergence to the southern Amazon ($\Delta\langle \overline{vq} \rangle_{sth}$) is computed from

$$\Delta\langle \overline{vq} \rangle_{sth} = \frac{(\langle \overline{vq} \rangle_{20°S,35°W–70°W} - \langle \overline{vq} \rangle_{6°S,35°W–70°W})/\Delta x_{35°W–70°W}}{\Delta y_{6°S–20°S}}, \quad (6)$$

where $\langle \overline{vq} \rangle_{20°S,35°W–70°W}$, $\langle \overline{vq} \rangle_{6°S,35°W–70°W}$, $\Delta x_{35°W–70°W}$, and $\Delta y_{6°S–20°S}$ are illustrated in Fig. 15. The total moisture convergence ($\Delta\langle \overline{\mathbf{V}q} \rangle_{sth}$) is the sum of $\Delta\langle \overline{uq} \rangle_{sth}$ and $\Delta\langle \overline{vq} \rangle_{sth}$. Figure 16b shows that $\Delta\langle \overline{\mathbf{V}q} \rangle_{sth}$ becomes convergent in September, the same month when the lower troposphere becomes more humid as shown in Fig. 6a, preceding the beginning of the wet seasons in October. The moisture divergence (negative) begins in April and peaks in June, 1 month ahead of the annual change of f_{DCC} (Fig. 16a). Hence, the changes in large-scale moisture convergence are apparently in phase with the lower-tropospheric moistening and so lead the onset of convection in the southern Amazon Basin. Therefore, the initial moisture changes appear to be the cause, rather than the result, of the wet season.

Figure 16b also shows that the zonal flux provides moisture largely from the eastern lateral boundary. But the annual changes of $\Delta\langle \overline{\mathbf{V}q} \rangle_{sth}$ are dominated by those of $\Delta\langle \overline{vq} \rangle_{sth}$, as determined by the meridional flux at 6°S, resulting from annual changes of the meridional wind. As shown in Fig. 12, lower-tropospheric winds near 6°S are strongly southeasterly in July (Fig. 12a) but are weakened in October (Fig. 12b). Such meridional divergence is overcome by zonal convergence in October. Hence, changes of circulation prior to the onset of the

wet seasons in the southern Amazon Basin force enhanced moisture convergence and promote convection.

In the equatorial Amazon, moisture converges to the region all year and with relatively small amplitude. Since the assimilated rainfall by the GEOS-1 is more uniformly distributed annually compared to the observations (similar problem exists in the NCEP reanalyses), we expect that the assimilated seasonal changes of moisture convergence are weaker and more temporally widespread than what they would be in reality. Perhaps as a result of this problem, the observed wet seasons do not correlate to maximum total moisture convergence. In the western equatorial Amazon (Fig. 17), total moisture convergence ($\Delta\langle\overline{\mathbf{V}q}\rangle_{\text{weq}}$) is almost invariant because of the balance between changes in $\Delta\langle\overline{uq}\rangle_{\text{weq}}$ and $\Delta\langle\overline{vq}\rangle_{\text{weq}}$ (Fig. 18b). However, f_{DCC} changes semiannually (Fig. 17a) with an amplitude similar to that in the southern Amazon. Here $\Delta\langle\overline{uq}\rangle_{\text{weq}}$ and $\Delta\langle\overline{vq}\rangle_{\text{weq}}$ are calculated by

$$\Delta\langle\overline{uq}\rangle_{\text{weq}} = \frac{(\langle\overline{uq}\rangle_{70^\circ\text{W},4^\circ\text{N}-6^\circ\text{S}} - \langle\overline{uq}\rangle_{60^\circ\text{W},4^\circ\text{N}-6^\circ\text{S}})/\Delta y_{4^\circ\text{N}-6^\circ\text{S}}}{\Delta x_{60^\circ\text{W}-70^\circ\text{W}}} \tag{7}$$

$$\Delta\langle\overline{vq}\rangle_{\text{weq}} = \frac{(\langle\overline{vq}\rangle_{6^\circ\text{S},60^\circ\text{W}-70^\circ\text{W}} - \langle\overline{vq}\rangle_{4^\circ\text{N},60^\circ\text{W}-70^\circ\text{W}})/\Delta x_{60^\circ\text{W}-70^\circ\text{W}}}{\Delta y_{4^\circ\text{N}-6^\circ\text{S}}}, \tag{8}$$

where the terms on the right-hand side of formulas (7) and (8) are illustrated in Fig. 15.

In the eastern equatorial Amazon, the GEOS-1 assimilation gives a semiannual cycle, instead of the observed annual cycle, of precipitation between 40° and 60°W, suggesting that its seasonal cycle of the moisture transport may not be reliable in detail for this region. Figure 18 shows that $\Delta\langle\overline{\mathbf{V}q}\rangle_{\text{eeq}}$ is more variable in the eastern than in the western equatorial Amazon and peaks from January through April. Here f_{DCC} (Fig. 18a) peaks during the season of maximum $\Delta\langle\overline{\mathbf{V}q}\rangle_{\text{eeq}}$ but lasts for a shorter period. Also, $\Delta\langle\overline{\mathbf{V}q}\rangle_{\text{eeq}}$ is dominated by zonal moisture convergence $\Delta\langle\overline{uq}\rangle_{\text{eeq}}$ in austral spring and by meridional moisture convergence $\Delta\langle\overline{vq}\rangle_{\text{eeq}}$ in austral fall. These two terms are computed by

$$\Delta\langle\overline{uq}\rangle_{\text{eeq}} = \frac{(\langle\overline{uq}\rangle_{60^\circ\text{W},4^\circ\text{N}-6^\circ\text{S}} - \langle\overline{uq}\rangle_{35^\circ\text{W},4^\circ\text{N}-6^\circ\text{S}})/\Delta y_{4^\circ\text{N}-6^\circ\text{S}}}{\Delta x_{35^\circ\text{W}-60^\circ\text{W}}} \tag{9}$$

$$\Delta\langle\overline{vq}\rangle_{\text{eeq}} = \frac{(\langle\overline{vq}\rangle_{6^\circ\text{S},35^\circ\text{W}-60^\circ\text{W}} - \langle\overline{vq}\rangle_{4^\circ\text{N},35^\circ\text{W}-60^\circ\text{W}})/\Delta x_{35^\circ\text{W}-60^\circ\text{W}}}{\Delta y_{4^\circ\text{N}-6^\circ\text{S}}}, \tag{10}$$

where the terms on the right-hand side of formulas (7) and (8) are illustrated in Fig. 15. Figures 12b (October) and 12d (April) suggest that the peak of $\Delta\langle\overline{uq}\rangle_{\text{eeq}}$ in austral spring results from a southeasterly flow from the Atlantic Ocean to the basin at 35°W and the peak of $\Delta\langle\overline{vq}\rangle_{\text{eeq}}$ in austral fall from a northeasterly flow at the equator and a southeasterly flow at 6°S.

In summary, Figs. 6–11 and 12–18 suggest that changes in the large-scale circulation are required to initiate the wet season in the tropical Amazon. In the southern Amazon, this is accomplished by transporting moisture into the region and destabilizing the inversion at the top of the PBL. In the equatorial Amazon, when moisture converges to the region horizontally throughout the year, the large uncertainties in the moisture transport make it difficult to quantify its role in determining seasonal variations in lower tropical humidity. The analysis period includes two El Niños (1987 and 1992/93) and one La Niña (1989). These interannual changes and also changes of SSTs over the Atlantic Ocean influence the frequency of convection (Figs. 13 and 14) and the details of the vertical thermodynamic structure (not shown). However, the temporal patterns of the seasonal cycles are still similar between the El Niño years and non–El Niño years. Hence, the above interannual changes more likely affect the amount of precipitation and the timing of the wet season rather than change the processes that control the onset of the wet season.

4. Discussion

a. The direct control by the large-scale circulation

A moistening of the lower troposphere and a destabilization of the inversion lead to the seasonal onset of convection in both the southern and the equatorial Amazon (Fig. 5). We suggest that these changes result from

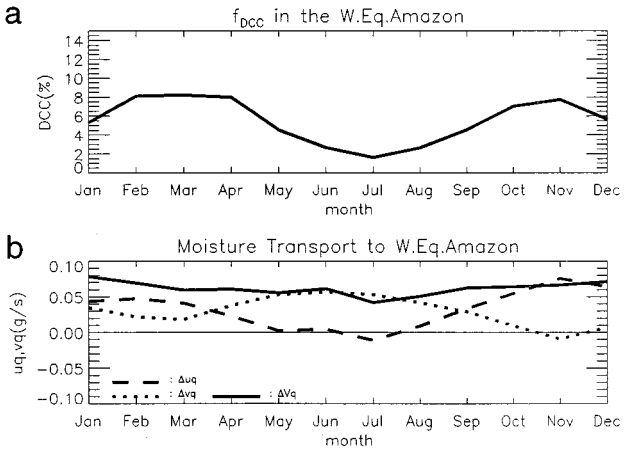

FIG. 17. As in Fig. 16 but for the western equatorial Amazon.

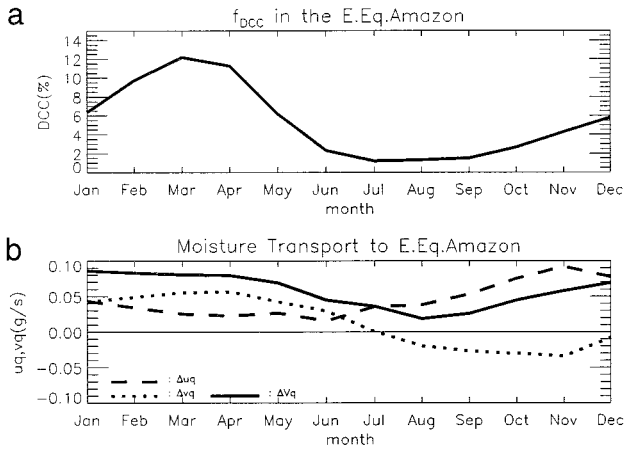

FIG. 18. As in Fig. 17 but for the eastern equatorial Amazon.

the increase of low-level moisture convergence rather than the increase of moisture and sensible heat fluxes at land surface for the following reasons. The moistening starts within the layers of atmosphere above the daily maximum PBL. Prior to the wet season, the inversion is strong and PBL is relatively well isolated from the above free atmosphere. The seasonal changes of surface evapotranspiration are smaller than those of low-level moisture convergence by a factor of 10, according to GEOS-1 reanalyses and ARME in situ observations. In the southern Amazon where the seasonal cycle of the moisture transport appears to be reliable, the moisture convergence is in phase with the moistening of the lower troposphere shown by radiosonde profiles and over one month leads the onset of the wet season. At Manaus, the surface evapotranspiration increases from May to September, but the moistening starts after August, one month after the low-level moisture convergence starts to increase (Fig. 17b). The moisture is evidently transported mainly in the free atmosphere and then entrained into the PBL during its growth from morning to early afternoon, as suggested by our analyses with a PBL model based on the ABLE and ARME observations. The destabilization is initiated by surface warming but continues after this warming ceases. The lapse rate does not become unstable until the cooling above the PBL occurs. During the austral spring, this period of relatively high frequency of DCC in the western basin has surface temperatures that are about the same as, or even lower than, those in the relatively dry eastern basin. But the lower troposphere is more humid and has no inversion so that a much greater frequency of convection occurs in the western basin at that time. Evidently, the changes in the atmospheric circulation that result in the these changes have more direct control over the thermodynamic structure, and hence the onset of the wet seasons than does the surface warming.

While this study suggests that the changes in large-scale atmospheric circulation are needed to establish the humid and unstable conditions for the onset of the wet season, it is still unclear what drives those circulation changes prior to the onset of large-scale convection. Numerical model simulations (e.g., Lenters and Cook 1997) suggest that latent heat released by convection is required to establish the Bolivian high with reasonable magnitude. Hence, the changes of the circulation throughout the deep troposphere associated with the Bolivian high may enhance the rainfall through its interaction with convection during the wet season but cannot initiate the wet season. Garreaud and Wallace (1998) have suggested that the low-level jets along the east side of the Andes transport higher θ_e and positive relative vorticity and hence lead the midlatitude intrusion of synoptic disturbances to the subtropical and tropical Amazon. A case study of an organized mesoscale convective complex during the ABLE 2B (Cohen et al. 1995) also suggests that the system is guided by a zonally orientated low-level jet that penetrates from the Atlantic to the western equatorial Amazon. They suggest that the moisture and perhaps also vorticity transport by low-level jets may be responsible for the initiation of the wet season.

b. The indirect influence of the land surface temperature

Although seasonal changes of land surface temperatures do not directly affect the onset of convection (Figs. 6–11), they are probably responsible for changes in circulation and so indirectly affect the onset of convection. In the southern Amazon, the radiosonde data (Fig. 6) show that the surface warming is followed first by a moistening in the lower and middle troposphere, then by cooling between 900 and 850 mb. Hence, we suggest that surface warming strengthens temperature gradients between the land and ocean and so causes the changes in circulation, perhaps in the lower troposphere, which in turn lead to the moistening and destabilization of the lower troposphere. In addition, surface warming also directly destabilizes the lapse rate in the lower tro-

posphere by more than 50% of that needed for the onset of convection. Hence, the land surface warming must still be an underlying, although indirect, driving force for the seasonal onset of convection in the southern Amazon.

The seasonal changes of surface temperatures in the equatorial Amazon are no more than 50% of those in the southern Amazon. The small local land surface temperature changes that peak at the onset of convection in austral fall have little direct effect on the static instability. The sea surface temperatures (SSTs) in the equatorial Atlantic and eastern Pacific reach their annual maximums in austral fall, but surface temperatures in the southern Amazon are cooler. Hence, there is a noticeable contrast between the warm zone between the equator and 10°S and the land and oceans farther south. Consequently, a lower-level wind convergence is established. Thus, the changes of large-scale circulation, which directly influence the onset of convection, are most likely driven by the changes in surface temperatures in remote land and oceanic regions. The observed relationships between convection and local surface conditions cannot be applied alone in the assessment of the sensitivity of convection to the changes in land surface conditions. Rather, changes in surface temperature gradients must also be considered.

c. *Why the onset of convection appears more sensitive to the land surface changes in the equatorial Amazon than in the southern Amazon*

Amplitudes of the annual changes of surface temperature (Fig. 14a) and humidity (Fig. 14b) in the equatorial Amazon are only about 25%–50% as much as those in the southern Amazon (Figs. 13a and 13b), but the changes in f_{DCC} and $Z_{200\mathrm{mb}}$ are as large as those in the southern basin (Figs. 13c and 14c). Why f_{DCC} appears to be more sensitive to the surface changes in the equatorial Amazon is explored by comparing the changes of the vertical thermodynamic structure between the dry and wet seasons at Vilhena and Manaus (Fig. 19). In January (Fig. 19a), the profiles of θ_e and θ_{es} are similar between two stations. On average, the atmosphere is unstable and the LFC at 1400 LT would be near 850 mb, as inferred from the near-surface θ_{es} calculated by the simple PBL model. Since the typical height of the PBL is about 880 mb during wet seasons near Manaus (Browell et al. 1990), convection can be easily initiated by organized dynamic disturbances or the turbulence in the PBL when it is deeper than its average height. Because the average atmospheric instability is very similar between the equatorial and southern central Amazon during the wet season, it is reasonable to expect a similar probability of occurrence of DCC, as observed by satellites (Figs. 13 and 14). The July atmosphere is very stable in the southern central Amazon, as shown by the profiles of θ_e and θ_{es} at Vilhena (Fig. 19b). Conversely, the atmosphere in the equatorial Amazon is sufficiently unstable above the boundary layer for the occurrence of convection, but the LFC at 1400 LT would be at 800 mb, 50 mb above the top of the daily maximum PBL (Martin et al. 1988). The winter circulation pattern apparently also suppresses organized low-level lifting so that most dynamic or turbulent disturbances cannot overcome the initial resistance to develop into deep convection. Hence, convection in the equatorial Amazon in July is discouraged by a large CINE rather than by a lack of tropospheric instability.

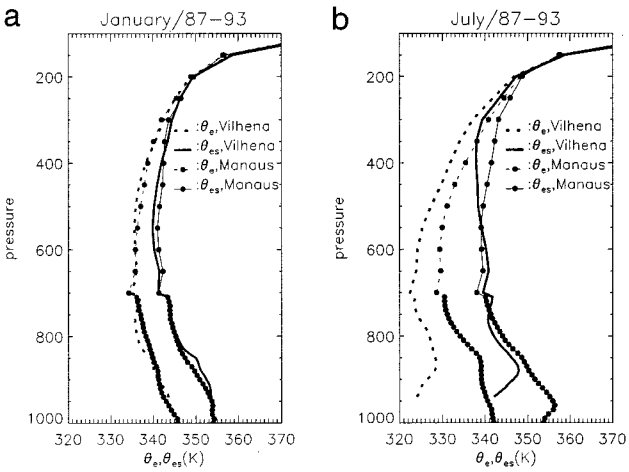

FIG. 19. (a) Profiles of θ_e (dashed curve) and θ_{es} (solid curve) of Jan averaged over the period of 1987–93 for Vilhena and Manaus (with dots). (b) As in (a) but for Jul.

Sections 4b and 4c suggest that the sensitivity of convection to changes in surface conditions depends on how stable the basic state of the system is. The atmosphere in the southern Amazon is very stable during the dry season and so requires a large increase of surface temperature and humidity to reach convective instability. By contrast, in the equatorial Amazon, convection is suppressed only by a stability barrier between the surface and 800 mb. Small changes are enough to break this barrier. This high sensitivity implies that the prediction of convection and precipitation in the equatorial Amazon requires more precise simulations of small changes in the atmospheric thermal and dynamic structures, especially in the PBL. In addition, changes in surface temperatures in the adjacent oceans also need to be considered; local surface conditions alone are likely to be poor predictors of the future occurrence of convection and precipitation in this region.

5. Conclusions

Although the wet season in the tropical Amazon (10°N–20°S) at any one place and in any one year is initiated rapidly by synoptic systems, this study shows that, probabilistically, the seasonal onset of convection in the Amazon Basin responds to changes in the thermodynamic structure as characterized by f_{CUS} and

CINE. To the south, where convection peaks in austral summer, the f_{CUS} and the reduction of CINE are both required for this seasonal onset. Near the equator, the frequency of convection increases starting in austral spring and reaches its maximum during austral fall (March and April) in the western equatorial Amazon. The long periods of convection in the western Amazon are encouraged by the weakening of CINE, which allows more disturbances to grow, but to the east with similar variations of CINE the lower f_{CUS} in spring suppresses convection such that the wet season is confined to austral fall. The local land surface temperature changes increase f_{CUS}. But the moistening in the PBL and cooling at the top of the PBL further reduce CINE. The enhancement of low-level convergence brings in more moisture into the region, leads to a more humid entrainment at the top of the PBL, and consequently moistens the PBL. Hence, the changes in the large-scale circulation dominate the moistening and cooling above the boundary layer and so provide the conditioning needed for the seasonal onset of convection.

In the southern Amazon, the atmosphere is very stable during the dry season but is no less unstable than the equatorial Amazon during the wet seasons. Surface warming destabilizes the lower-tropospheric lapse rate from July to September. From October to December, surface temperatures decrease, but more moisture is transported into the region from the equator, with a net moisture convergence and a moistening of the lower troposphere. Following this, a moistening of the PBL and cooling at the top of the PBL occurs, and the frequency of convection increases from less than 5% to more than 10%. The seasonal changes of atmospheric circulation cause this moistening and cooling and therefore directly control the onset of convection. The land surface warming, however, increases f_{CUS} and the gradient of land–ocean temperature and so is the primary driver of seasonal changes of circulation.

In the equatorial Amazon, the moistening of the PBL and the absence of inversion associated with changes in the large-scale circulation increase the probability of convection and promote the onset of wet season. The annual changes of the local land surface temperature are only 25%–50% of those in the southern Amazon. The changes of large-scale circulation are probably driven by SSTs in the equatorial Atlantic and eastern Pacific and by land surface temperatures in the southern Amazon. The local land surface temperature changes are less important to the seasonal changes of convection relative to those in the southern Amazon.

The temporal patterns of the seasonal cycles of convection and the vertical thermodynamic profiles are similar between the El Niño years and non–El Niño years. Hence, the interannual changes of SSTs in the tropical Pacific and Atlantic Oceans more likely affect the amount of precipitation and the timing of the wet season rather than change the processes that control the onset of the wet season. While this study suggests that changes in the large-scale circulation are needed to establish the suitable thermodynamic conditions for the wet seasons, what drives these needed changes has not been addressed here.

Acknowledgments. This study was supported by the Pan American Climate Study Program of the NOAA Global Office (NA56GP0232-01), a National Science Foundation grant (NSF ATM 9419715), and the New Investigator Program of the National Aeronautics and Space Administration Earth Observing System. We thank the NASA/Langley DAAC and Data Assimilation Office for freely providing ISCCP B3 and GOES-1 reanalyses datasets, NCAR Data Support Center for the global radiosonde data, Mingxiang Chen for her computational help, and Margaret Sanderson Rae and Cas Sprout for editorial assistance.

REFERENCES

Betts, A. K., 1973: Non-precipitating cumulus convection and its parameterization. *Quart. J. Roy. Meteor. Soc.*, **99,** 178–196.

Bolton, D., 1980: The computation of equivalent potential temperature. *Mon. Wea. Rev.*, **108,** 1046–1053.

Browell, E. V., R. C. Harriss, and V. W. J. H. Kirchhoff, 1990: Ozone and aerosol distributions over the Amazon Basin during the wet season. *J. Geophys. Res.*, **95,** 16 887–16 901.

Chu, P. S., 1985: A contribution of the upper-air climatology of tropical South America. *J. Climatol.*, **55,** 403–416.

Cohen, J. C. P., M. A. F. Silva Dias, and C. A. Nobre, 1995: Environmental conditions associated with Amazonian squall lines: A case study. *Mon. Wea. Rev.*, **123,** 3163–3174.

Eltahir, A. B., and J. S. Pal, 1996: Relationship between surface conditions and subsequent rainfall in convective storms. *J. Geophys. Res.*, **101,** 26 237–26 245.

Figueroa, S. N., P. Satyamurty, and P. L. Silva Dias, 1995: Simulations of the summer circulation over the South American region with an eta coordinate model. *J. Atmos. Sci.*, **52,** 1573–1584.

Fitzjarrald, D. R., and M. Garstang, 1981: Boundary-layer growth over the tropical ocean. *Mon. Wea. Rev.*, **109,** 1762–1772.

Fu, R., A. D. Del Genio, and W. B. Rossow, 1990: Behavior of deep convective clouds in the tropical Pacific deduced from ISCCP radiances. *J. Climate*, **3,** 1129–1152.

——, ——, and ——, 1994: Deep convection, vertical thermodynamic structure, and surface conditions in the tropical Pacific. *J. Climate*, **7,** 1092–1108.

Gaffen, D., 1996: A digitized metadata set of global upper-air station histories. NOAA Tech. Memo. ERL ARL-211, 38 pp.

Garreaud, R. D., and J. M. Wallace, 1998: Summertime incursions of midlatitude air into subtropical and tropical South America. *Mon. Wea. Rev.*, **126,** 2713–2733.

Garstang, M., and Coauthors, 1990: The Amazon Boundary-Layer Experiment (ABLE 2B): A meteorological perspective. *Bull. Amer. Meteor. Soc.*, **71,** 19–32.

——, H. L. Massie Jr., J. Halverson, S. Greco, and J. Scala, 1994: Amazon coastal squall lines. Part I: Structure and kinematics. *Mon. Wea. Rev.*, **122,** 608–622.

Greco, S., and Coauthors, 1990: Rainfall and surface kinematic conditions over central Amazonia during ABLE 2B. *J. Geophys. Res.*, **95,** 17 001–17 014.

Harriss, R. C., and Coauthors, 1988: The Amazon Boundary Layer Experiment (ABLE 2A): Dry season 1985. *J. Geophys. Res.*, **93,** 1351–1360.

——, and Coauthors, 1990: The Amazon Boundary Layer Experiment: Wet season 1987. *J. Geophys. Res.*, **95,** 16 721–16 736.

Hastenrath, S., 1997: Annual cycle of upper air circulation and con-

vective activity over the tropical Americas. *J. Geophys. Res.*, **102,** 4267–4274.

Horel, J. D., A. N. Hahmann, and J. E. Geisler, 1989: An investigation of the annual cycle of convective activity over the tropical Americas. *J. Climate*, **2,** 1388–1403.

James, I. N., and D. L. T. Anderson, 1984: The seasonal mean flow and distribution of large-scale weather systems in the southern hemisphere: The effects of moisture transport. *Quart. J. Roy. Meteor. Soc.*, **110,** 943–966.

Jones, C., and B. Weare, 1993: A time series analysis of evaporation and wind speed over the Amazon Basin. Preprints, *Fourth Symp. on Global Change Studies,* Anaheim, CA, Amer. Meteor. Soc., 423–426.

Kagano, M. T., 1979: Um estudo climatológico e sinótico utilizando dados de radiossondagem de Manaus e Belém. M.S. thesis, INPE-1559-TDL/013, São Jose de Campos, Brazil, 82 pp.

Knutson, T. R., and K. M. Weickmann, 1987: 30–60 day atmospheric oscillations: Composite life cycles of convection and circulation anomalies. *Mon. Wea. Rev.*, **115,** 1407–1436.

Kousky, V. E., 1988: Pentad outgoing longwave radiation climatology for the South American sector. *Revista Bras. Meteor.,* **3,** 217–231.

Kreuels, R., K. Fraedrich, and E. Ruprecht, 1975: An aerological climatology of South America. *Meteor. Rundsch.,* **28,** 17–24.

Lenters, J. D., and K. H. Cook, 1997: On the origin of the Bolivian high and related circulation features of the South America climate. *J. Atmos. Sci.*, **54,** 656–677.

Marengo, J. A., 1992: Interannual variability of surface climate in the Amazon Basin. *Int. J. Climatol.,* **12,** 853–863.

Martin, C. L., D. Fitzjarrald, M. Garstang, A. P. Oliveira, S. Greco, and E. Browell, 1988: Structure and growth of the mixing layer over the Amazonian rain forest. *J. Geophys. Res.,* **93,** 1361–1375.

Neelin, J. D., 1997: Implications of convective quasi-equilibrium for the large-scale flow. *The Physics and Parameterization of Moist Atmospheric Convection,* R. K. Smith, Ed., Kluwer Academic, 413–446.

Nishizawa, T., and M. Tanaka, 1983: The annual change in the tropospheric circulation and the rainfall in South America. *Arch. Meteor. Geophys. Bioklmatol.,* **33,** 107–116.

Rao, V. B., I. F. A. Cavalcanti, and K. Hada, 1996: Annual variation of rainfall over Brazil and water vapor characteristics over South America. *J. Geophys. Res.*, **101,** 26 539–26 551.

Rossow, W. B., and R. A. Schiffer, 1991: ISCCP cloud data products. *Bull. Amer. Meteor. Soc.,* **72,** 1–20.

Schubert, S. D., J. Pfaendtner, and R. Rood, 1993: An assimilated dataset for earth science applications. *Bull. Amer. Meteor. Soc.,* **74,** 2331–2342.

Schwerdtfeger, W., 1961: Strömungs-und temperaturfeld der freien atmosphäre uber den Anden. *Meteor. Rundsch.,* **14,** 1–6.

Shuttleworth, W. J., 1988: Evaporation from Amazonian rainforest. *Proc. Roy. Soc. London.*, **233B,** 321–346.

Tennekes, H., 1973: A model for the dynamics of the inversion above a convective boundary layer. *J. Atmos. Sci.,* **30,** 558–567.

Velasco, I., and J. M. Fritsch, 1987: Mesoscale convective complexes in the Americas. *J. Geophys. Res.,* **92,** 9591–9613.

Virji, H., 1981: A preliminary study of summertime tropospheric circulation patterns over South America estimated from cloud winds. *Mon. Wea. Rev.,* **109,** 599–610.

Williams, E., 1991: Comments on ''Thunderstorms above frontal surfaces in environments with positive CAPE. Part I: A climatology.'' *Mon. Wea. Rev.,* **119,** 2511–2513.

——, and N. Rennó, 1993: An analysis of the conditional instability of the tropical atmosphere. *Mon. Wea. Rev.,* **121,** 21–36.